Static and Seismic Analysis of the Janneh Arch-gravity Dam

Theme B – 14th International Benchmark Workshop on the Numerical Analysis of Dams

Gracia L. [1], de-Pouplana I. [1], Salazar F. [1] and Oñate E. [1,2]

[1]*CIMNE – Centre Internacional de Metodes Numerics en Enginyeria, Gran Capitán s/n, 08034 Barcelona, SPAIN*

[2]*Departament d'Enginyeria Civil I Ambiental (ECA), Universitat Politècnica de Catalunya (UPC), Campus Nord, Edif. C1, C. Jordi Girona, 1-3, 08034 Barcelona, SPAIN*

E-mail: lgracia@cimne.upc.edu

ABSTRACT: The static and seismic analysis of Janneh arch-gravity dam (157 m) is carried out by considering a combination of self-weight, hydrostatic, uplift and seismic loads. Linear and nonlinear analyses are performed for both static and seismic cases. Nonlinear behavior is studied by means of joint elements in the contact between the rock foundation and the dam following a bilinear cohesive law. The hydrodynamic effects derived to seismic loads are also considered. Hydrodynamic Westergaard's approach is applied in the pseudo-static analysis, and the Westergaard's generalized added mass is used for time-history case.

1 Introduction

Earthquakes are considered one of the main causes that activate mechanisms leading to dam failure (e.g Fujinuma Dam, which failed because of Tōhoku earthquake on March of 2011) or damage.

Thereby, in the context of the theme B of the 14th ICOLD Benchmark Workshop on Numerical Analysis of Dams [1], the present work has the object of verifying the Janneh arch-gravity dam under a static and seismic load scenarios. Before performing both analyses, a simulation of the constructive phase is carried out with the aim of obtaining the residual stresses at this early stage. The nonlinear analysis is performed using joint elements allowing the joint opening in the contact area between dam body and foundation. The uplift pressure is also considered when nonlinear analysis is performed since the thickness of the dam is relatively high. Seismic analysis is performed through a dynamic analysis using a Newmark time integration scheme [2] and a viscous damping of 5%, and also a massless foundation [3]. Hydrodynamic effects are considered using the Westergaard's approach in the pseudo-static analysis and the Westergaard's generalized mass [4] for time-history analysis.

An open source C++ FEM framework called Kratos Multiphysics [5] is used for solving the proposed problem. The pre and processing simulations are performed with GiD [6], which has been previously employed in the design [7] and analysis [8] of arch dams. The paper is organized as follows. First, the essential theory and formulation is introduced, including the activation process, interface elements used, time integration scheme and the formulation of hydrodynamic effects, and then the numerical model is described along with the most representative results.

2 Formulation

2.1 Activation process

The methodology for solving the constructive phase is based on a layer by layer activation process. The contribution of each layer is activated (and considered) according to the construction process. This is the initial state for assessing the stress state of the dam. During this process, only gravitational forces are considered – the thermal load is neglected.

2.2 Joint elements

Joint elements (or interface elements) are special elements that allow representing discontinuities in the displacement field. -They are versatile and suitable to simulate contact opening. They are designed to transmit both compressive and tensile stresses; the latter are governed by a cohesive constitutive law (Figure 1), which is very common in fracture mechanics [9]. One of the most important differences with respect to the standard finite elements is that the quantities of interest in the interface elements are computed in local coordinates, i.e. normal and tangential relative displacements need to be handled. Figure 1 relates the normalized equivalent stress ς_{eq} with the internal historical state variable ι, and shows that the evolution of the cohesive zone is an irreversible damage process.

Figure 1: Bilinear cohesive law.

This internal historical state variable characterizes the maximum strain level reached in the previous history of the material up to given time t:

$$\iota(t) = \min\left\{\max\left\{\iota_y, \max_{\tau \le t} \varepsilon_{eq}(\tau)\right\}, 1\right\} \tag{1}$$

In equation (1), ι_y is the damage threshold (or yield strain), and ε_{eq} is the equivalent strain computed in local coordinates through the tangential and normal relative displacements:

$$\varepsilon_{eq} = \frac{\sqrt{\epsilon_l^2 + \epsilon_m^2 + \epsilon_n^2}}{\epsilon_c} \tag{2}$$

with ϵ_c being the critical displacement, i.e. the relative displacement at which the cohesive zone stops transmitting forces. The normalized equivalent stress can be defined as:

$$\varsigma_{eq} = \frac{\sqrt{(\sigma'_l)^2 + (\sigma'_m)^2 + (\sigma'_n)^2}}{\sigma_y} \qquad \sigma'_l = \frac{\sigma_y(1-\iota)}{\iota\epsilon_c(1-\iota_y)}\epsilon_l \qquad \sigma'_m = \frac{\sigma_y(1-\iota)}{\iota\epsilon_c(1-\iota_y)}\epsilon_m \qquad \sigma'_n = \frac{\sigma_y(1-\iota)}{\iota\epsilon_c(1-\iota_y)}\epsilon_n \tag{3}$$

where σ_y is the yield stress, i.e. the stress at which the cohesive zone starts damaging. When there is contact between the two faces of an interface, the equivalent strain is computed just

from the tangential relative displacements and the tangential stresses are defined like the shear strength of the Mohr-Coulomb criterion:

$$\varepsilon_{eq} = \frac{\sqrt{\epsilon_l^2 + \epsilon_m^2}}{\epsilon_c} \qquad |\sigma_l'| = |c_l| + \mu_F |\sigma_n'| \qquad |\sigma_m'| = |c_m| + \mu_F |\sigma_n'| \tag{4}$$

With this approach, damage threshold and yield stress govern the contact opening between dam body and foundation. A high value of yield stress represents a monolithic behavior at the contact area.

2.3 Integration Scheme

An implicit Newmark-beta time integration scheme is used [2]. Values of $\gamma = 0.5$ and $\beta = 0.25$ have been chosen in order to achieve stability, leading to the constant average acceleration method [2]. Also, the selection of $\gamma = 0.5$ provides second order accuracy method. The linearization of the momentum equation using the displacements as the unknowns leads to the following linear equation:

$$K_{t+\Delta t}^{*i} \Delta U_{t+\Delta t}^{i+1} = R_{t+\Delta t}^{i} \tag{5}$$

where

$$K_{t+\Delta t}^{*i} = K_t + \frac{\gamma}{\beta \Delta t} C_t + \frac{1}{\beta \Delta t^2} M \tag{6}$$

and

$$R_{t+\Delta t}^{i} = F_{t+\Delta t}^{ext} - F(U_{t+\Delta t}^{i-1})^{int} - C\dot{U}_{t+\Delta t}^{i-1} - M\ddot{U}_{t+\Delta t}^{i-1} \tag{7}$$

γ and β are the aforementioned parameters of the time integration scheme, Δt is the time step, $K_{t+\Delta t}^{*i}$ corresponds to left hand side contribution composed by: the stiffness matrix K_t, the damping matrix C_t and the mass matrix M_t, $\Delta U_{t+\Delta t}^{i+1}$ is the vector of incremental displacements, and $R_{t+\Delta t}^{i}$ is the right hand side contribution composed by: external forces $F_{t+\Delta t}^{ext}$, internal forces $F(U_{t+\Delta t}^{i-1})^{int}$, the contribution of vector velocities $C\dot{U}_{t+\Delta t}^{i-1}$ and accelerations $M\ddot{U}_{t+\Delta t}^{i-1}$ at previous step.

2.4 Hydrodynamic effects

In a linear pseudo-static analysis, an extra hydrodynamic force is added to the model according to Westergaard's approach. The hydrodynamic force follows the direction of the inertial forces, i.e. -when the inertial load is applied in the upstream direction, the hydrodynamic force also follows that direction, neutralizing the hydrostatic force.

Regarding time-history analysis, Westergaard's added mass is used for both linear and nonlinear analyses. It enables to represent the inertia of the fluid on the structure during earthquake. The Westergaard's distribution (8) applied at each node is proportional to a surface density of mass computed as:

$$f(z) = \frac{7}{8} \times \rho_w \times \sqrt{H \times (z_0 - z)} \tag{8}$$

Where ρ_w is the fluid density, H the water depth, z_0 the water surface elevation and z the elevation of the node under consideration. This contribution is added to the real mass of the dam increasing the total mass of the system.

3 Numerical model

A mesh of linear tetrahedrons is used for both static and dynamic analyses, with a mean size of 3 m for the dam body and 25 m for the foundation. The resultant mesh has 117K nodes and 654K elements (Figure 2), almost 500K are concentrated in the dam body.

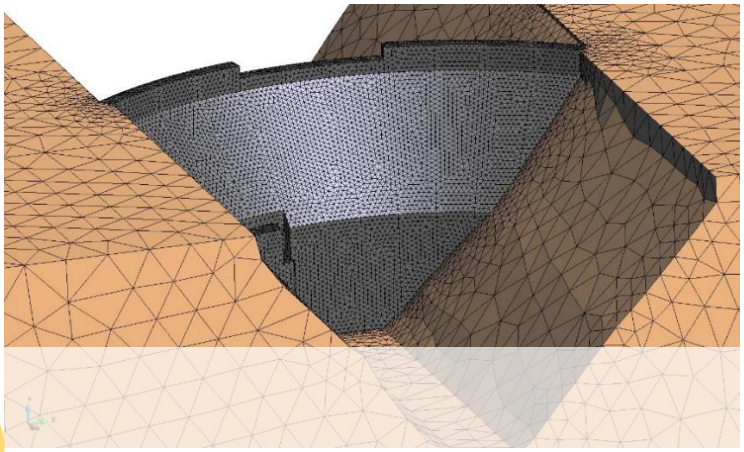

Figure 2: Computational mesh.

The material properties are presented in Table 1. In case of seismic analysis the bedrock is considered massless according to the problem statement.

Table 1: Material Properties.

Property	Bedrock	Dam	Joint	Units
Density (ρ)	2.8e3	2.4e3	2.4e3	kg/m^3
Static Young's modulus (E)	2.5e10	2.0e10	2.0e10	N/m^2
Dynamic Young's modulus (E)	3.0e10	3.0e10	3.0e10	N/m^2
Poisson's ratio (ν)	0.25	0.2	0.2	-
Min. Joint Width (δ_{min})	-	-	5e-03	m
Critical displacement (ϵ_c)	-	-	0.05	m
Yield stress (σ_y)	-	-	3.0e8 - 2.0e10*	N/m^2
Damage threshold (ι_y)	-	-	0.35	-
Friction coefficient (μ)	-	-	0.4	-

* In self-weight, static and dynamic linear analysis, the value of yield stress is set to 2.0e10 N/m^2 in order to prevent the joint opening and represent that the dam is attached to the foundation, while in nonlinear cases the value is set to 3.0e8 N/m^2 allowing its opening.

Seismic analyses are performed using the dynamic Young's modulus. Table 2 shows the load combination for each scenario.

Table 2: Load scenarios.

Analysis	Loads
Self-weight	Gravitational force (G)
Static Linear	Hydrostatic force (H)
Static Nonlinear	Hydrostatic force + Uplift pressure (U)
Pseudo-Static Nonlinear	H + U + Inertial load + Hydrodynamic force
Dynamic Linear	H + Inertial load + Hydrodynamic Added mass
Dynamic Nonlinear	H + U + Inertial load + Hydrodynamic Added mass

4 Results

4.1 Self-weight Analysis

A layer by layer activation procedure is used to simulate the constructive process. The dam body is built in 16 stages, each of which activates a layer of 10 meters. Figure 3 shows the dam at two different stages.

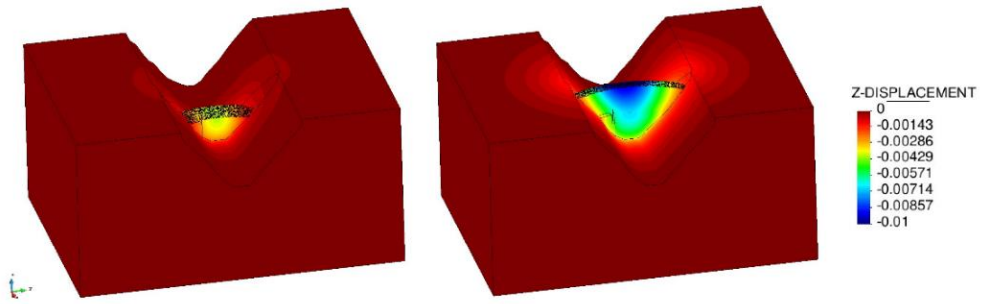

Figure 3: Constructive phase. Left: Stage 6 (60 m). Right: Stage 12 (120 m).

The stress field after the constructive phase is used as an initial stress state for the remaining analyses, while the strains associated to the construction are neglected. Minimum principal stresses (compression) at the downstream and upstream face are presented in Figure 4.

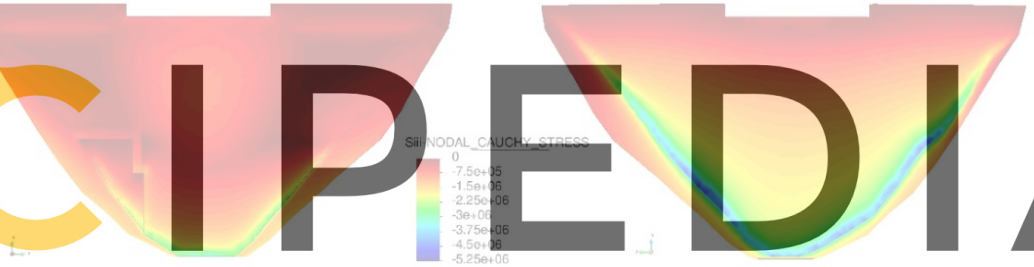

Figure 4: Contour plots of principal compressive stresses after construction. Views from downstream (left) and upstream (right).

4.2 Static Analysis

Linear Analysis

The water level of the reservoir is 149m (hydrostatic load) and the downstream water level is at the bedrock level. In order to ensure a monolithic behavior, a high value of yield stress (2.0e10 N/m^2) is assigned to the joint element in this scenario. Displacement-X at blocks B0 and B5 (Figure 5) are plotted versus the elevation in Figure 6. In the case of block B0 it coincides with radial displacements, with a maximum value of 1.8 cm at the top of the dam.

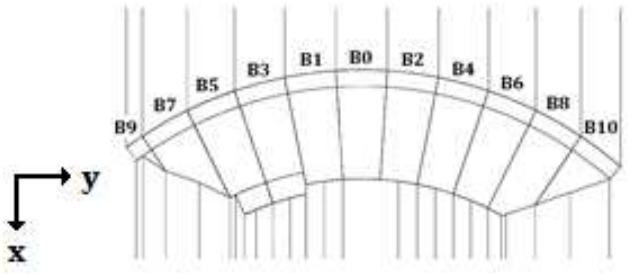

Figure 5: Block numbering of Janneh dam.

Simplified Nonlinear Analysis

In this scenario, the uplift pressure is considered and its effect on dam-foundation contact opening evaluated. Figure 6 shows the evolution of the displacement-X at B0 and B5 versus the elevation considering these assumptions (the value of yield stress is 3.0e8 N/m^2).

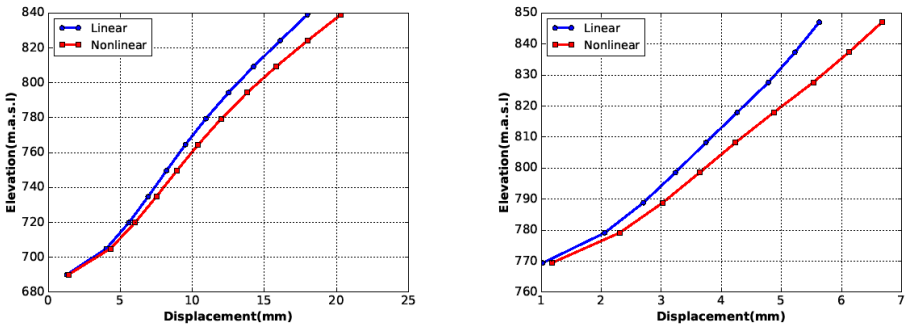

Figure 6: Displacement-X vs. elevation at Block B0 and B5.

The results of the nonlinear analysis show an increment on the maximum displacements of around 12% with respect to the linear ones in the static case. The main cause of such increments is the inclusion of the uplift pressure as well as the influence of the joint opening.

Figure 7 shows the evolution of the joint opening along the thickness of the dam at the center of block B0 and at the interface between block B3 and B5. The maximum values are 0.10 and 0.18 mm respectively. This increment is due to the particular geometry of that zone.

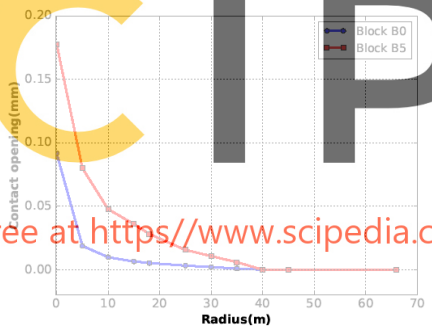

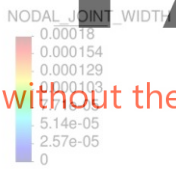

Figure 7: Joint Opening. Left: Contact opening vs. radius. Right: Section at center of B0 block and B3-B5 block.

To obtain the acting forces at dam/foundation interfaces of blocks B0 and B5, the stress at each element is multiplied by its area to compute the elemental forces. Such force is transformed into global coordinates and all elemental contributions in the interface are accumulated. Finally, the total force in the interface is rotated to obtain the normal and tangential components at the plane of interest.

4.3 Seismic Analysis

An Eigenvalue problem must be solved to obtain the natural frequencies of the dam. The modal analysis is performed using the dynamic properties of the materials. In the computation of the fundamental frequencies, the influence of the reservoir is not included. It is well known that its consideration leads to smaller frequencies, increasing the natural period [10].

Table 3: Natural frequencies and periods.

Mode	ω (rad/s)	Frequencies (Hz)	Period (s)	% Mass
1	29.504	4.696	0.213	18.1
2	38.948	6.199	0.161	1.1

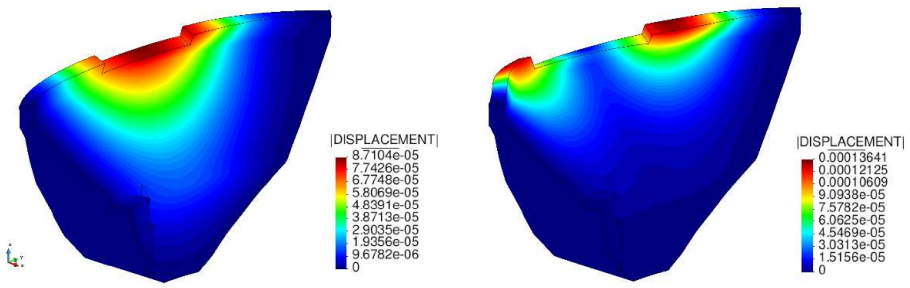

Figure 8: Contour plots of the Displacement-X. Left: 1st mode. Right: 2nd mode.

Non Linear pseudo-static analysis based on the site response spectrum

The period for the first frequency is 0.213s and according to the site response spectrum acceleration for a 5% damping, the corresponding acceleration is 8.78m/s^2. Hydrodynamic forces are computed using the Westergaard´s approach. Positive and negative acceleration are considered as well as the influence of the uplift pressure. Figure 9 presents a sketch of the applied forces.

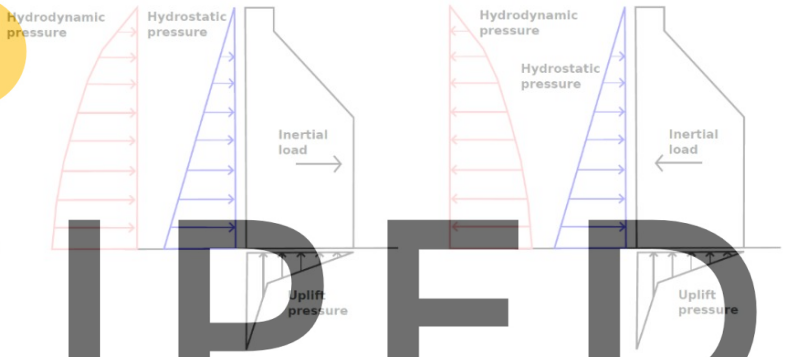

Figure 9: Load combinations for pseudo-static analysis Left: Upstream-Downstream direction. Right: Downstream-Upstream direction.

The load combinations prescribed above are the most unfavorable ones according to the input acceleration. The use of Westergaard's approach as an external load can lead to conservative results. Nonetheless, thanks to the pseudo-static analysis it is possible to obtain the maximum displacements rank. Figure 10 shows a comparison of displacement-X versus elevation at block B0 and B5 (S-L = Static Linear, S-NL = Static Nonlinear, PS-UPS-DW = Pseudo-static inertia upstream-downstream, PS-DW-UPS = Pseudo-static inertia downstream-upstream).

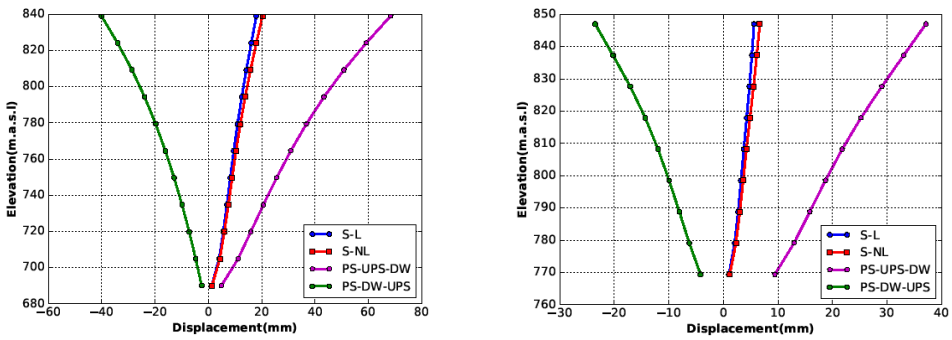

Figure 10: Displacement-X vs. elevation at block B0 and B5.

Table 4 presents the maximum displacement-X value reached in each simulation as well as the arch stress at level 737.0 of block B0. In the case of upstream direction a positive value of 1.40MPa at level 737.0 is reached. Figure 11 shows the displacement-X field for both combinations.

Table 4: Nonlinear pseudo-static results.

Inertial Load	B0 Disp-X (mm)	B5 Disp-X (mm)	Arch Stress at B0 737.0 level (MPa)
Downstream	68.32	30.93	-3.88
Upstream	-40.04	-21.35	1.40

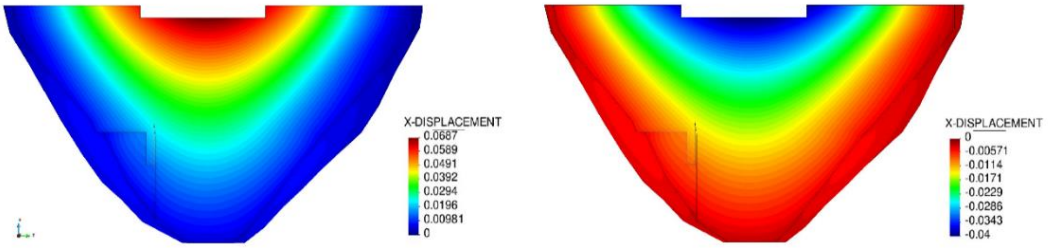

Figure 11: Contour plots of the Displacement-X. Left: Downstream Inertia Load. Right: Upstream Inertia Load.

Linear time-history analysis with simplified dynamic interactions

A linear model is used at this stage, thus dam/foundation interface behavior is monolithic. The set of loads are: hydrostatic pressure, hydrodynamic pressure and a set of accelerograms in horizontal and vertical directions which are imposed as volume forces, representing the earthquake accelerations. The hydrodynamic contribution is considered via the generalized Westergaard's added mass previously introduced.

Nonlinear time-history analysis with simplified dynamic interactions

A nonlinear analysis is performed through the usage of joint elements and the consideration of the uplift pressure (steady). The results are compared to linear time-history analysis with -and without hydrodynamic to highlight the influence of the reservoir in the structural response.

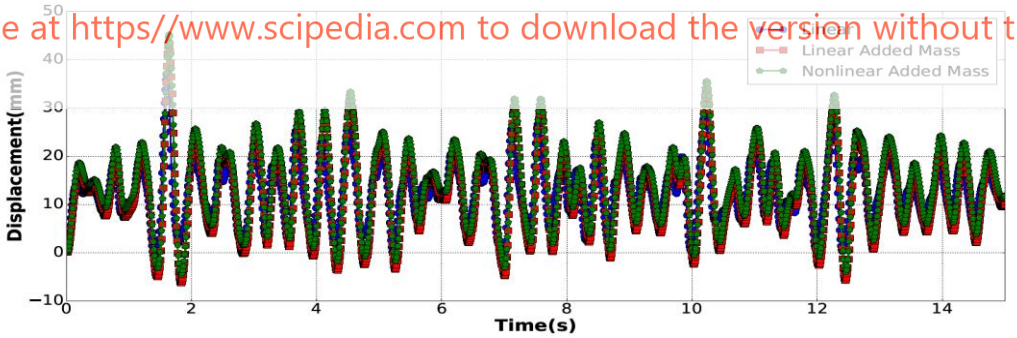

Figure 12: Displacement-X at the top of block B0.

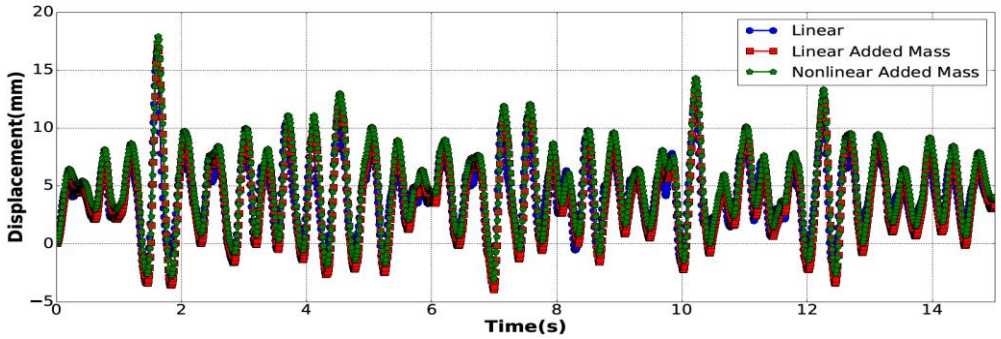

Figure 13: Displacement-X at the top of block B5.

Figures 12 and 13 show the evolution of displacement-X at the top of blocks B0 and B5, respectively. The influence of the reservoir increases the maximum and minimum values throughout the simulation. The consideration of the added mass increases around 15% the maximum value of displacements. Nonlinear analysis shows an increment of maximum values of over 6% due to the influence of uplift pressure and the joint opening. It is important to note that the minimum values are smaller because the joint closes when the acceleration changes direction. Figures 14 and 15 shows the measured module of accelerations at the top of block B0 and B5 at center. Both simulations show that the accelerations are smaller due to the increment of mass. Nonetheless, such addition of mass does not change the structural behavior. Similar results are obtained in linear and nonlinear cases with added mass.

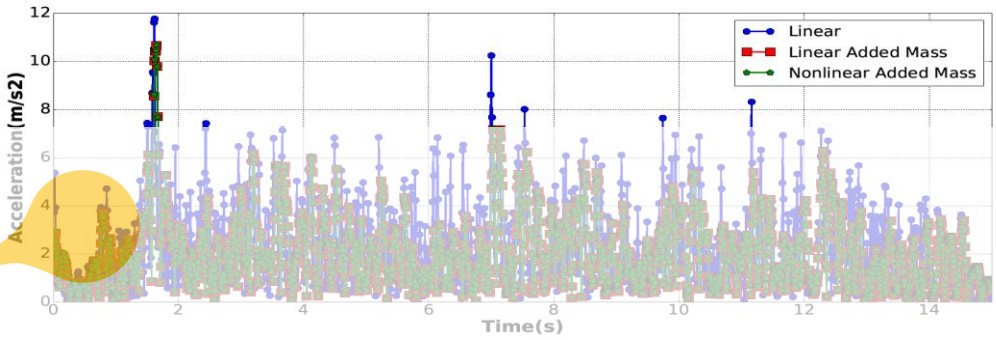

Figure 14: Module of accelerations at center of block B0.

Figure 15: Module of accelerations at center of block B5.

Finally, the time history of arch stress at elevation 779.0 of block B0 is presented in Figure 16. The minimum value is reached when the maximum value of acceleration acts, -3.5MPa.

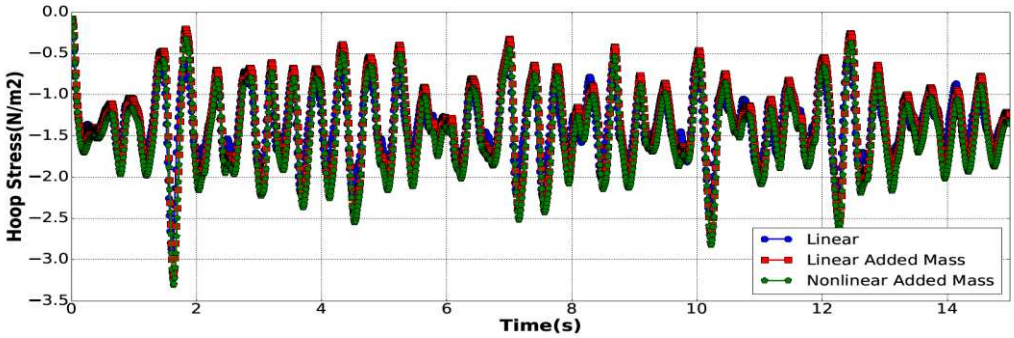

Figure 16: Hoop Stress at block B0 at 779 m.a.s.l.

In all time-history simulations it can be appreciated a delay between the input seismic load and its response due to the influence of the viscous damping of 5%. This effect is more remarkable when the added mass is used.

5 Conclusions

A linear and nonlinear finite element static and dynamic analysis of a concrete arch-gravity dam has been performed with the following conclusions:

- Results show the effect of the uplift pressure, which is relevant in the case study due to relatively high base thickness (67m).
- The joint elements allow considering the opening of the dam-foundation contact, although calibration of their constitutive parameters is required.
- The pseudo-static analysis provides useful information on dam behavior, though the range of displacements is over estimated.
- The hydrodynamic effect considered through Westergaard's added mass increases the maximum values of displacements in up to a 15%. The consideration of a compressible reservoir can lead to accurate results but, given the high stiffness of the dam, the expected variation is small.
- The results confirm that the increment of dam thickness is adequate to improve dam response to earthquakes.

In the authors' opinion, the numerical tools used in the present work can be effectively used to predict and analyse the nonlinear response of dams to seismic loads. However, calibration of the model parameters is necessary to obtain more reliable results in quantitative terms.

6 Acknowledgements

We acknowledge the financial support to CIMNE via the CERCA Programme / Generalitat de Catalunya. The research was also supported by the Spanish Ministry of Economy and Competitiveness (Ministerio de Economía y Competitividad, MINECO) through the projects ACOMBO (RTC-2015-3794-5) and NUMA (RTC-2016-4859-5).

7 References

[1] Andrian F., Agresti P. and Mathieu G. (2017). 14th Benchmark Workshop on the Numerical Analysis of Dams, ICOLD Committee on Computational Aspects of Analysis and Design of Dams.
[2] Newmark, N.M. (1959). A Method of Computation for Structural Dynamics. ASCE Journal of Engineering Mechanics Division, Vol 85. No EM3.
[3] Chopra A. (2012). Earthquake Analysis of Arch Dams: Factors to Be Considered, Journal of Structural Engineering, vol. 138, pp. 205-214.
[4] Westergaard H. M. (1933). Water Pressure on Dams during Earthquakes. Transactions, ASCE, Vol. 98, 418-472.
[5] Kratos Multiphyisics. http://www.cimne.com/kratos/, June 2017.
[6] GiD the personal pre and post processor. http://www.gidhome.com/, June 2017.
[7] Vicente, D.J., San Mauro, J., Salazar, F. and Baena, C.M. (2017). An Interactive Tool for Automatic Predimensioning and Numerical Modeling of Arch Dams. Mathematical Problems in Engineering, vol. 2017, Article ID 9856938, doi:10.1155/2017/9856938
[8] Salazar, F., Toledo, M. Á., González, J. M., and Oñate, E. (2017). Early detection of anomalies in dam performance: A methodology based on boosted regression trees. Struct. Control Health Monit., doi: 10.1002/stc.2012.
[9] Camacho G. T. and Ortiz. M. (1996). Computational modelling of impact damage in brittle materials. International Journal of Solids and Structures, 33(20):2899–2938.
[10] Mosquera, J. C. (1995). Efectos hidrodinámicos en el análisis sísmico de presas bóveda. Ingeniería del agua, vol. 2, no 1.